LASER INTERFEROMETER GRAVITATIONAL WAVE OBSERVATORY
- LIGO -
CALIFORNIA INSTITUTE OF TECHNOLOGY
MASSACHUSETTS INSTITUTE OF TECHNOLOGY

Technical Note LIGO-T1500427-v1 2015/09/25

Experimental Study of Crackling Noise as Micro-mechanics of Flow

Kla Karava
Mentors: Xiaoyue Ni, Rana Adhikari, Julia R. Greer

Distribution of this document:
LIGO Scientific Collaboration

California Institute of Technology
LIGO Project, MS 18-34
Pasadena, CA 91125
Phone (626) 395-2129
Fax (626) 304-9834
E-mail: info@ligo.caltech.edu

Massachusetts Institute of Technology
LIGO Project, Room NW17-161
Cambridge, MA 02139
Phone (617) 253-4824
Fax (617) 253-7014
E-mail: info@ligo.mit.edu

LIGO Hanford Observatory
Route 10, Mile Marker 2
Richland, WA 99352
Phone (509) 372-8106
Fax (509) 372-8137
E-mail: info@ligo.caltech.edu

LIGO Livingston Observatory
19100 LIGO Lane
Livingston, LA 70754
Phone (225) 686-3100
Fax (225) 686-7189
E-mail: info@ligo.caltech.edu

Kla Karava[1,*]
Mentors: Xiaoyue Ni[2], Rana Adhikari[2], Julia R. Greer[3]

[1] Department of Physics, University of Cambridge, Cambridge, United Kingdom
[2] LIGO Laboratory, California Institute of Technology, Pasadena, California, United States
[3] Division of Engineering and Applied Sciences, California Institute of Technology, Pasadena, California, United States

Abstract

In crystalline materials, dislocation dynamics can generate strain noise upon being applied by rapidly-changing, oscillatory stress in the elastic regime. This so-called crackling noise may arise inside the maraging steel blades of the quadruple pendulum which serves as the suspension system of the Advanced LIGO. The study focuses on the nature and origin of crackling noise in metals. Monocrystalline copper nanopillars are used as model system for this purpose. Sinusoidal load perturbation to quasi-static compressive loading was applied to copper nanopillars with different system sizes, and the loss and storage moduli were measured as function of static stress. Amorphous fused silica nanopillars were also studied as to eliminate non-dislocation-dynamics effects. It was found that the loss moduli, which characterise the energy dissipation mechanism of the system, are not constant throughout the static, elastic loading in copper; we also observed size-dependence of this anomalous dynamic mechanical behaviour. Our results confirm a deviation from the perfectly elastic behaviour which can further indicate intermittent dislocation dynamics as the source of crackling noise.

1. Introduction and Background

1.1 Motivation for Crackling Noise in Crystalline Materials

In 1919, Heinrich Barkhausen discovered magnetisation is a discrete process rather than being perfectly continuous [1]. In other words, when we look closely at a magnetisation curve (B-H curve), magnetic flux intensity (B) increases with applied magnetic field (H) in a ladder-like manner as shown in figure 1. These ladder-step variations are called *Barkhausen noise.* This noise originates from the intrinsic nature of magnetic dipoles inside magnetic materials.

Figure 1: a B-H curve with magnification to reveal the discrete nature [1]

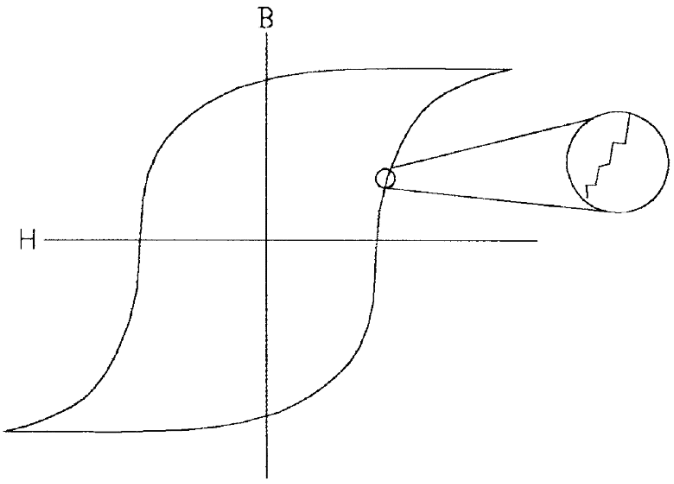

From this discrete nature magnetisation, an analogy could be made for crystalline materials in form of *mechanical strain noise.* A magnetisation curve (B-H curve) is to be replaced by a loading curve (stress-strain curve) and we would expect to observe similar ladder-like steps during loading. This postulated mechanical strain noise is commonly referred to as *crackling noise.*

1.2 Potential Crackling Noise in Advanced LIGO

Crackling noise may arise inside the *quadruple pendulum* that is used as the suspension system inside the Advanced LIGO [2]. The maraging steel blades are used for vertical seismic isolation [3]. However, since there is no spring-blade isolation between the upper intermediate mass and the test mass, crackling noise produced in the upper intermediate mass maraging steel blade could propagate directly into the test mass. This crackling noise profoundly limits the sensitivity of the detector in the seismic frequency range [4].

1.3 Non-linear Dislocation Interactions: Potential Sources of Crackling Noise

Dislocation mechanics is the major means of plastic deformation in crystalline materials. The planes of atoms in a crystal can move past one another once dislocation avalanches are activated (macro-plasticity). Since dislocations are usually pinned by defects or even by other dislocations, they can bow out under an application of shear stress that might be much smaller than the yield stress through the process called *Orowan bowing* [5]. In this sense, there can be dislocation dynamics inside the material (micro-plasticity) even though the bulk material is not plastically deformed. This would mean there could be some dislocation dynamics in the elastic regime.

The theoretical perspective on the relationship between viscoelasticity and collective dislocation dynamics is concisely provided by Laurson and Alava (2012) [6]. It was found from simulations that there are intermittencies in hysteresis loops when the amplitude and the frequency of the applied sinusoidal stress are varied. In this sense, dislocations can oscillate back and forth, and energy is dissipated. However, dislocation interactions induce a tendency to form dislocation multipoles with each multipole moving together [6]. The complex network of dislocations in the crystal can act non-linearly through long-range, coherent interactions between dislocations. Potential crackling noise in crystalline materials is *most likely* to be due to these non-linear, long-range interactions between dislocations. However, this is the result from pure computer simulations and there has not been any experimental confirmation yet.

2. Methods

2.1 Copper Nanopillars as Model System

The study of crackling noise in this project focuses on monocrystalline (single crystal) metals because polycrystalline metals are too complicated for any fundamental features of crackling noise, if exists, to be revealed evidently. For this purpose, pure copper is chosen as our model system in preference to maraging steel, which is the real metal used as the blades of the suspension system of the Advanced LIGO, because firstly, maraging steel is an alloy which means it contains various impurities while pure copper contains no impurity at all so that the true nature of dislocations can be revealed. Secondly, copper is a face-centred cubic (fcc) metal while maraging steel is a body-centred cubic (bcc) metal. Fcc metals have true close-packed slip planes but bcc metals do not [5]. This intrinsic difference means that dislocation mechanics is more preferable in fcc than bcc metals. There can be other competitive deformation mechanisms in bcc metals such as twinning. Therefore, choosing an fcc metal as model ensures that only dislocation mechanics takes part in. And lastly, copper (especially copper nanopillars) is more widely studied and documented [7].

In order to magnify the stochastic nature of dislocations, *nanopillars* are used in the study rather bulk materials. The *size-effect*, i.e. smaller (crystalline) systems behave differently from larger systems, takes part significantly at the sub-micron scales. The most well-known corollary of the size-effect is 'the smaller, the stronger' or in other words, smaller (crystalline) samples possess higher yield strength [7].

Copper nanopillars with diameter of 500 nm and height of 1500 nm (aspect ratio 1:3) were used primarily as model system in this study because they are easy to fabricate, widely studied, and sufficiently small to observe the stochastic nature.

In addition to 500 nm copper nanopillars, 1 μm copper nanopillars (aspect ratio 1:3) were also studied as to observe the transition of the behaviour, if any, into the real world situation where the materials are bulk.

2.2 Fabrication of Nanopillars: Focused Ion Beam (FIB)

The fabrication of nanopillars is conventionally done by the technique called *focused ion beam* or *FIB*. FIB is very similar to SEM but Ga^+ ions, instead of electrons, are shone onto the surface of a substrate and the material's meat is milled out. Greater details of FIB can be found in Latif (2000) [8] or Yao (2011) [9].

The FIB machine used in this project is *FEI™ Versa 3D™* that belongs to Greer's group at Caltech. The product data and specifications can be found in [10].

The workflow is as followed. Firstly, patterns comprising concentric rings are designed and tried until the desired dimensions of nanopillars are achieved. Larger diameter rings are associated with higher beam currents and smaller rings with lower currents. The specimen has to be milled out from larger to smaller rings because this is the best way to minimise redeposition of the milled debris, and also this method produces better nanopillars with sharper circumference and length. Next, the patterns are aligned manually in the software interface by the user. Then, the user will have to activate the FIB beam to mill out the specimen ring-by-ring at a given beam current (whether automatically or not depending on the design). These procedures are to be repeated for smaller, subsequent beam currents. Nanopillars are fabricated in batches with 9 nanopillars per batch. Lastly, the nanopillars in each batch are photographed using SEM and the dimensions are measured individually using the tool in the software.

2.3 Indirect Approach: Energy Dissipation

A naïve approach to prove the existence of crackling noise would be a direct look into the elastic region of a loading curve and see if strain increases in a ladder-like manner with stress or not. The problem is that with our current, direct measurements, the data are too noisy to reveal such postulated features. An example of the elastic regime of real load vs. displacement data of a 500 nm copper nanopillar using Hysitron TriboIndenter® is given in figure 2.

Figure 2: an elastic loading curve of a 500 nm copper nanopillar

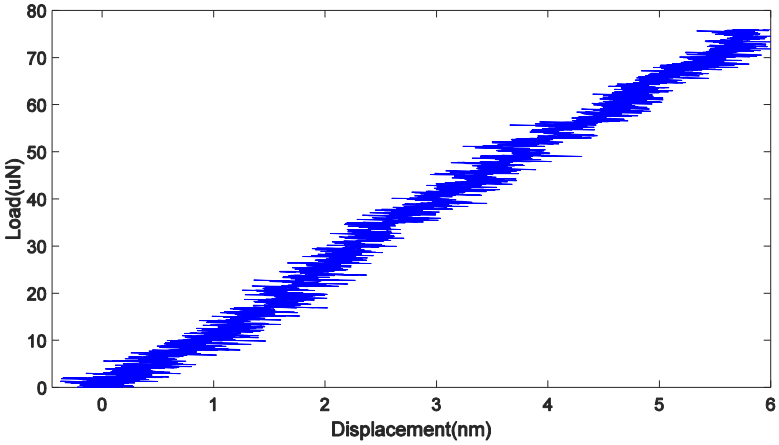

The most plausible alternative approach to direct detection is the *energy dissipation* approach. As discussed previously in section 1.3 of the report, the manifestation of the existence of dislocations in crystalline solids is mechanical energy dissipation or internal friction [6]. Sinusoidal stress were applied to the surface of copper nanopillars and the energy dissipation would be monitored to see if there was any deviation from the perfectly linear, elastic picture or not. This method is called *dynamic mechanical analysis* or *DMA*. This will be discussed in the next section.

2.4 Dynamic Mechanical Analysis (DMA)

Dynamic mechanical analysis or *DMA* is a method in materials science where sinusoidal stress is applied to a sample and sinusoidal strain response with the same angular frequency ω is returned and measured. The convention is that the applied stress leads the strain response by a phase of δ [5]. Stress and strain as functions of time are given in equations 1 and 2 respectively.

$$\sigma = \sigma_0 \sin(\omega t + \delta) \quad \text{(Eq.1)}$$

$$\varepsilon = \varepsilon_0 \sin(\omega t) \quad \text{(Eq.2)}$$

In experiment, sinusoidal stress is applied in *steps* with increasing *static stress*, i.e. the mean stress of each step, over the course of loading. This type of loading regime is called *step DMA*. This is best illustrated by an example of real load vs. time data shown in figure 3.

Figure 3: a trimmed section of a step DMA load function with frequency 1 Hz

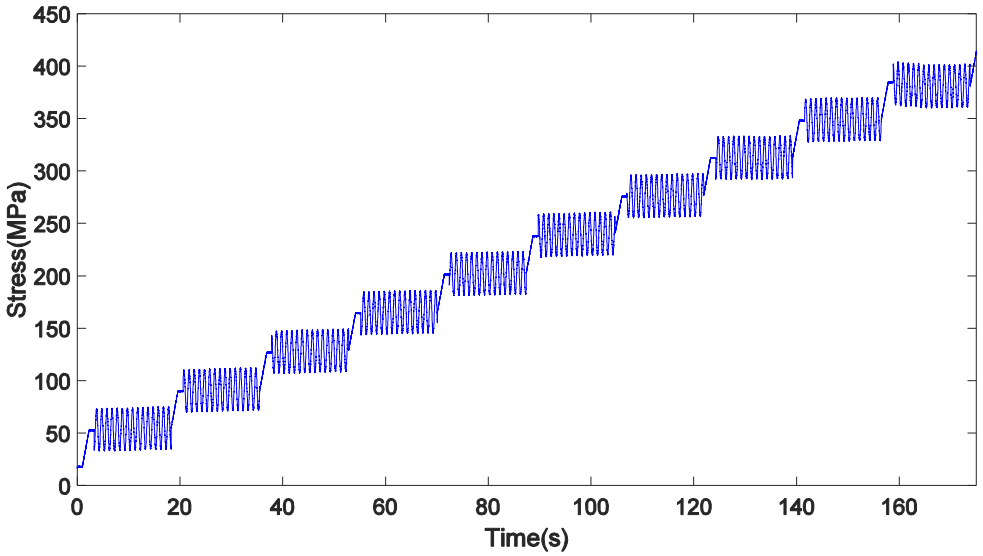

DMA tests on nanopillars were performed by a commercialised nanoidentation machine called *Hysitron TriboIndenter*®. This machine uses the patented 3-plate capacitor/transducer technology that provides simultaneous actuation and measurement of force and displacement [11]. A schematic cross-section of the transducer assembly is given in figure 4. Force is exerted on a specimen by varying the offset voltage given to the central plate of the 3-plate transducer [12]. The contact tip used in this experiment is an 8 µm diamond flat punch. All controls of the machine are made through the software provided by Hysitron. Details of how the TriboIndenter® works are beyond the scope of this report but the reader may find out more information in [11], [12], [13], and [14].

Figure 4: a schematic cross-section of the 3-plate transducer assembly of the TriboIndenter® [15]

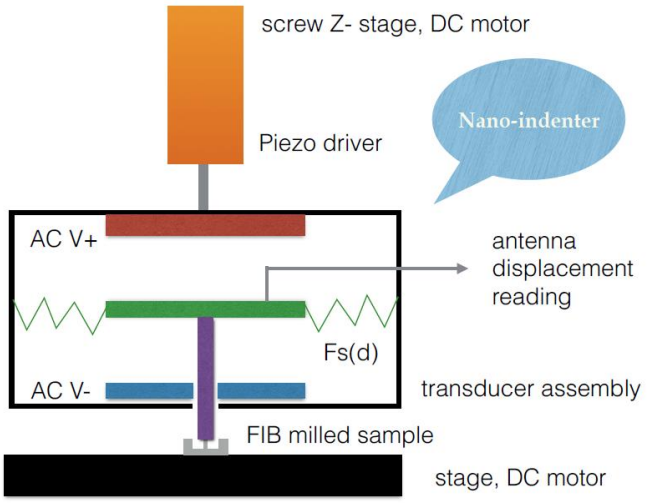

For each individual static step, *dynamic modulus* can be evaluated using the load and displacement data of that step. *Dynamic modulus (E)* is the ratio of stress and strain under oscillatory conditions and is a property of viscoelastic materials [5]. It is often expressed as a complex quantity with real part being *storage modulus* and imaginary part being *loss modulus*. This is expressed in equation 3.

$$E = E_{storage} + iE_{loss} \quad \text{(Eq.3)}$$

Storage modulus measures the energy stored in the viscoelastic material whereas loss modulus indicates the energy dissipated as heat.

For a uniaxial, sinusoidal load, storage and loss moduli are defined as:

$$E_{storage} = \frac{\sigma_0}{\varepsilon_0}\cos\delta \quad \text{(Eq.4)}$$

$$E_{loss} = \frac{\sigma_0}{\varepsilon_0}\sin\delta \quad \text{(Eq.5)}$$

where σ_0 is stress amplitude, ε_0 is strain amplitude, and δ is phase difference between stress and strain defined in equations 1 and 2. The complex modulus of dynamic modulus corresponds to conventional Young's modulus.

2.5 Continuous DMA

The resolution of the dynamic moduli vs. static stress plot can be highly enhanced by employing a continuous sinusoidal load so-called *continuous DMA*. Basically, the stress is linearly, continuously increased with time just like uniaxial compression tests; but now the line is modulated with a sinusoid so that the load function takes the form of a sloping sinusoid as shown in figure 5.

Figure 5: a trimmed section of a continuous DMA load function with frequency 1 Hz

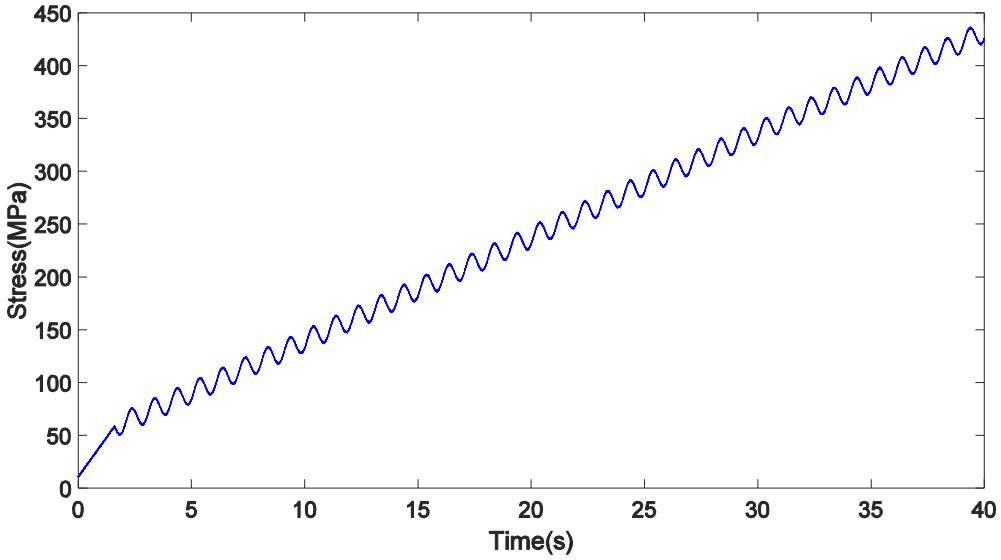

The static stress along the loading curve is represented by the moving-average values of the stress over a certain, specified interval of time. The *packet* of sinusoids associated with a certain value of moving-average static stress contains all the sinusoids that lie within a certain, specified interval. Then, the amplitude of this sinusoidal segment can be found by least-squared fitting.

2.6 Parameters of DMA

The parameters of a DMA test include the number of static steps, maximum load, begin amplitude, amplitude type, and frequency. The parameters could be adjusted for different pillars from different batches as to see if the results were different for different loading conditions or not.

The number of static steps merely determines the resolution of the moduli vs. static stress plots and does not affect the behaviour of the load data.

The amplitude of the load should affect the dynamical behaviour of the pillars since the dislocations inside the pillars experience different levels of stress for a given static stress step.

There are two types of load amplitude: linearly variable amplitude, and constant amplitude. Linearly variable amplitude ensures that the amplitude increases proportionally with static stress. Constant amplitude retains constant amplitude for all the static stress steps.

And lastly, the frequency of the AC load can be adjusted to see if the behaviour of dynamic moduli is frequency-dependent or not. The frequencies studied in this project are 1, 10, and 200 Hz. This project especially focuses on frequency 1 Hz because this is the frequency of seismic vibration which is pertinent to the disturbance of the Advanced LIGO. The environment created by DMA tests with frequency 1 Hz should replicate the real-world situation of seismic vibration.

Conventional *step* DMA tests were used for 1 Hz whilst *continuous* DMA tests were used for 10 and 200 Hz. The main reason for not using *continuous* DMA tests for 1 Hz is because the number of data points is not sufficient for proper moving-average sinusoid fitting so that the errors are larger than the case of *step* DMA tests.

Details regarding parameter selections and adjustments are discussed in section 3.4.

2.7 Standard Linear Model of Solids: Perfectly Elastic Picture

Wright *et al* (2007) [16] provides a rigorous analysis on the subject. Nanoidentation system can be modelled by the traditional Voigt solid model where a viscoelastic solid is represented by a spring (elastic portion) connected in parallel with a dashpot (viscous portion). This is schematically illustrated in figure 6.

Figure 6: a schematic representation of a nanoindenter [16]

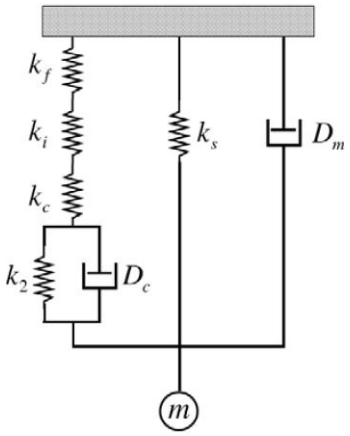

The elements of this model include k_f, frame stiffness; k_i, indenter stiffness; k_c, contact stiffness; k_2, material stiffness; k_s, leaf spring stiffness; D_c, contact damping; D_m, machine damping; and m, indenter column mass. k_f, k_i, k_c are in parallel to each other and the combined spring constant is referred to as k_1. The detail and meaning of each of the elements can be found in Wright *et al* (2007) [16].

From author's derivation based on the standard linear model, it is found that dynamic moduli are independent of static stress and are, therefore, constant throughout the elastic regime at constant frequency (see section 3.3.2). However, dynamic moduli are function of frequency. A brief derivation and appropriate equations are given in section A1 of the appendix.

2.8 Energy Dissipation Revisit

Mentioned earlier in section 2.3, we postulated that crackling noise is potentially originated from long-range interactions between dislocations. This means stress-strain hysteresis would change if there were these dislocation interactions [6]. Since the area bounded by hysteresis is the energy dissipated in a cycle, changes in the shape of hysteresis would mean loss moduli are not constant over the course of loading. Therefore, measuring loss moduli at different static stages in the elastic regime and plotting them as function of static stress to see if they are constant or not would testify our hypothesis. Changes in loss moduli over the elastic regime could be the sign of deviation from the perfectly linear, elastic behaviour .

Uniaxial compression tests were performed on a few first batches to serve as system benchmarks; Young's moduli were measured and used as reference. The elastic part of each of the dynamic moduli measured from the DMA test should agree well with the reference value. There were 8 pillars available for each batch for DMA tests since the first pillar was always used for a uniaxial compression test. The reason of doing this was to ensure that the tip was well-aligned and ready for more sensitive DMA tests afterwards.

2.9 Fused Silica Nanopillars

In order to ensure that any deviation from the standard linear model is due to intrinsic dislocation dynamics rather than other extrinsic causes such as machine artefacts, same experiment was also undergone on 500 nm fused silica nanopillars. The primary difference between copper and fused silica is that copper is crystalline whilst fused silica is amorphous. Being amorphous means that there is no dislocation present; consequently, this means there is no size-effect [7] so that DMA tests were performed on 500 nm nanopillars only. A different dynamical behaviour would be observed if our hypothesis of elastic dislocation mechanics were true.

3. Results and Discussion

3.1 Fabrication of Nanopillars

For 500 nm copper nanopillars, 16 batches were fabricated in total. There are 9 pillars per batch. An overview section of the surface of the copper substrate with a few working batches is shown in figure 7.

Figure 7: an overview of the surface of the copper substrate

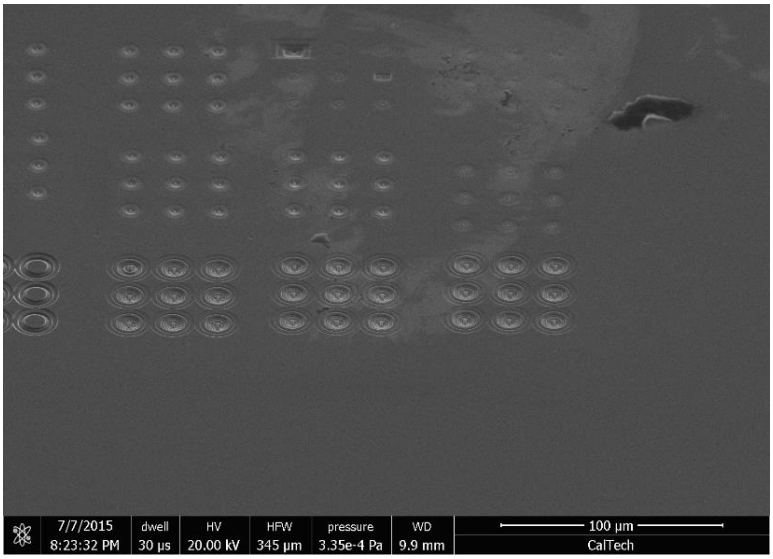

The fabricated nanopillars are never perfectly cylindrical. All nanopillars inevitably suffer from *tapering* of various degrees. Their shape is rather like a lampshade than a cylinder. Figures 8 and 9 show two 500 nm copper nanopillars of different degrees of tapering. Tapering is mainly caused by imperfect focusing and poor adjustments of the stigmator. This effect can be alleviated by good focus adjustment and stigmation of the FIB. It should be noted that the contact surface's diameter never achieves the nominal value of 500 nm.

Figure 8: a lightly tapered 500 nm copper nanopillar

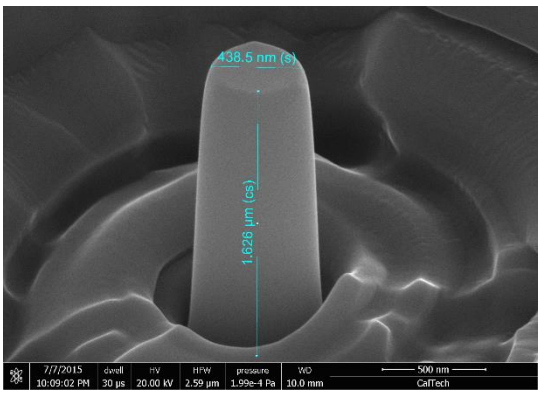

Figure 9: a severely tapered 500 nm copper nanopillar

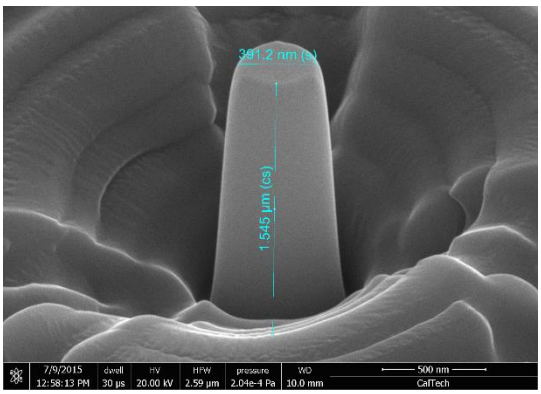

For 1 μm copper nanopillars, 4 batches were fabricated. However, tapering is much less pronounced for 1 μm nanopillars so that the actual diameter is close to the nominal value. An example of a 1 μm copper nanopillars is given in figure 10.

Figure 10: a 1 μm copper nanopillar

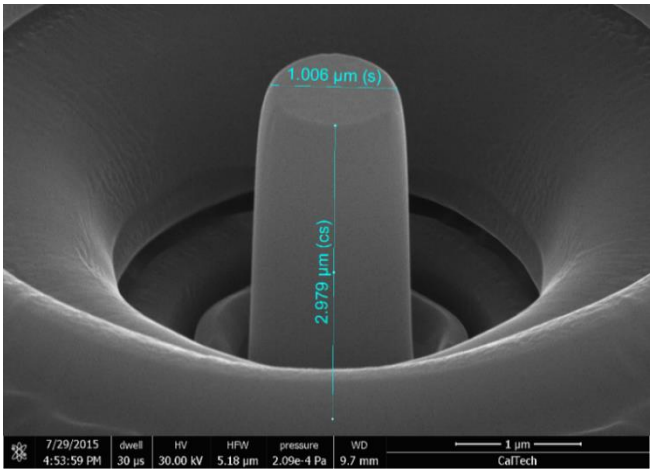

And lastly, for 500 nm fused silica nanopillars, 4 batches were fabricated. Tapering in fused silica is relatively better than that in 500 nm copper nanopillars. However, the mean diameter of the fabricated nanopillars is still less than the nominal value of 500 nm. An example is given in figure 11.

Figure 11: a 500 nm fused silica nanopillar

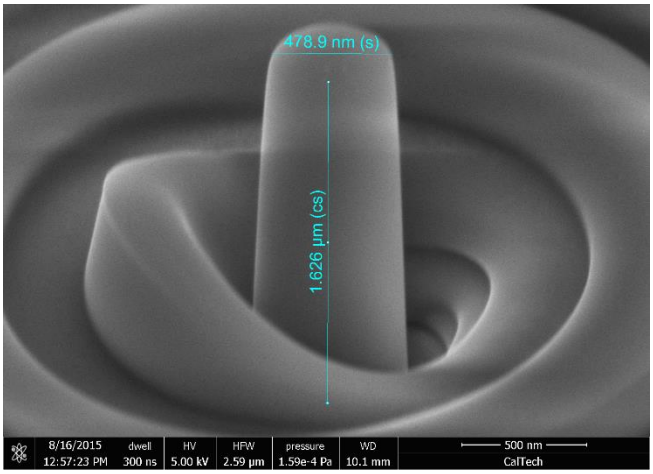

3.2 Uniaxial Compression Tests

3.2.1 500 nm Copper Nanopillars

For copper nanopillars, dislocation bursts after yielding are always expected to be observed. This phenomenon is a means of verifying that the indenter tip is properly aligned and thus, uniaxial compression is performed on the copper nanopillar instead of indentation. The loading rate was chosen to be such that the strain rate was as slow as 10^{-3} s^{-1}. A selected example of the load vs. displacement plot for proper uniaxial compression on a 500 nm copper nanopillar where dislocation bursts are evident is given in figure 12. And an example of indentation is given in figure 13.

Figure 12: a proper compression test on a 500 nm copper nanopillar with evident dislocation bursts

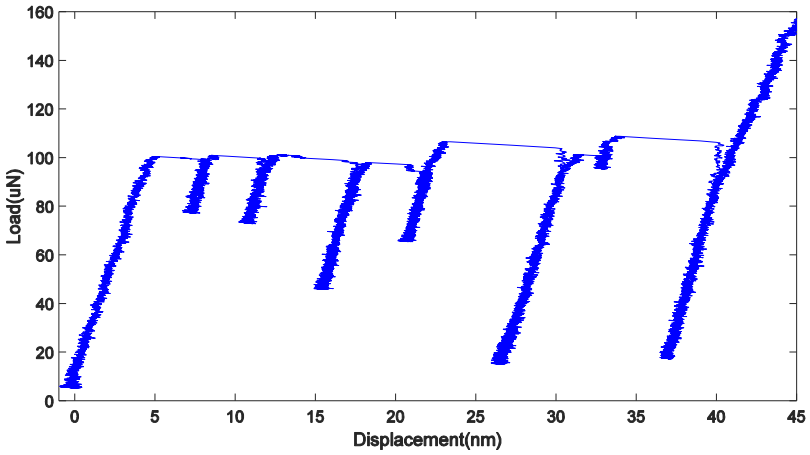

Figure 13: an indentation on a 500 nm copper nanopillar with no dislocation burst

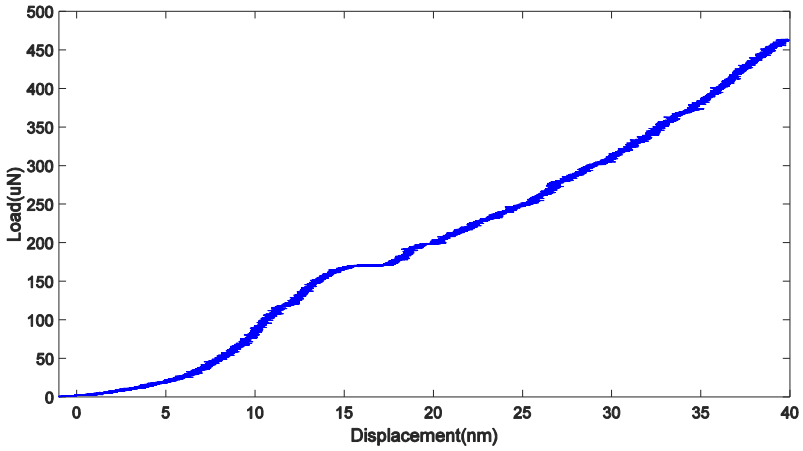

The Young's modulus and the yield strength for each pillar were found using a Matlab code developed by the author. The bases of the code are as followed. Firstly, the load and displacement data are converted into stress and strain respectively using the appropriate diameter and height of

the pillar. Young's modulus can be found from the slope of the linear, elastic line (depicted by the red line in figure 14). Yield stress is the maximum value of stress of the elastic regime. The convention of the yield point is the point of intersection between the line of 0.2% plastic strain [17] (depicted by the green line in figure 14) and the stress-strain curve.

Figure 14: the stress vs. strain plot cropped to show only the elastic regime for a uniaxial compression test on a 500 nm copper nanopillar

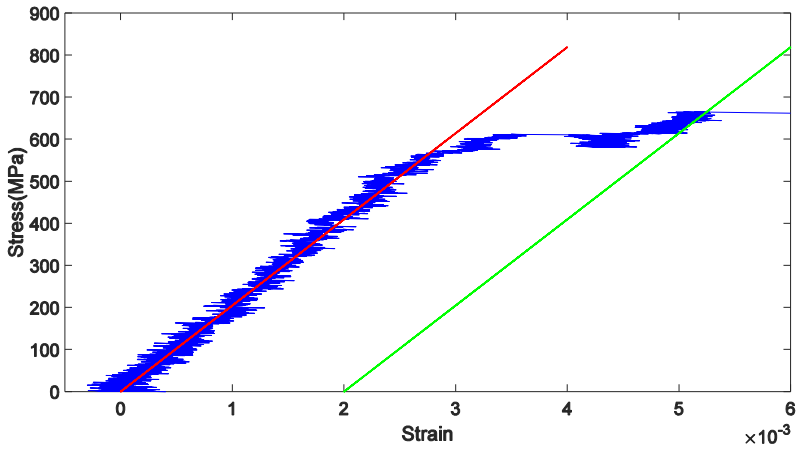

Uniaxial compression tests were performed on the first 3 batches and the first pillar of each of the following batches. The summary of results for 500 nm copper nanopillars is provided in table 1 below. For Young's modulus, the experimental value of 150 GPa, is considerably larger than the reference value of 138 GPa [18]. For yield strength, the reference value is 400 MPa is for 500 nm copper nanopillars [19], [20]. However, due to tapering, the mean diameter reduces to 442 nm which then means that the yield strength is expected to be higher due to the size-effect [7], [20]. Hence, the value of 539 MPa is reasonable.

Table 1: results for compression tests on 500 nm copper nanopillars

Young's modulus(GPa)	150 ± 8
Yield strength(MPa)	539 ± 25
Diameter(nm)	442 ± 11
Height(nm)	1580 ± 30

3.2.2 1 µm Copper Nanopillars

Uniaxial compression tests were performed on 1 batch of 1 µm copper nanopillars. A selected stress-strain curve cropped to show only the elastic regime is shown in figure 15.

Figure 15: the stress vs. strain plot cropped to show only the elastic regime for a uniaxial compression test on a 1 µm copper nanopillar

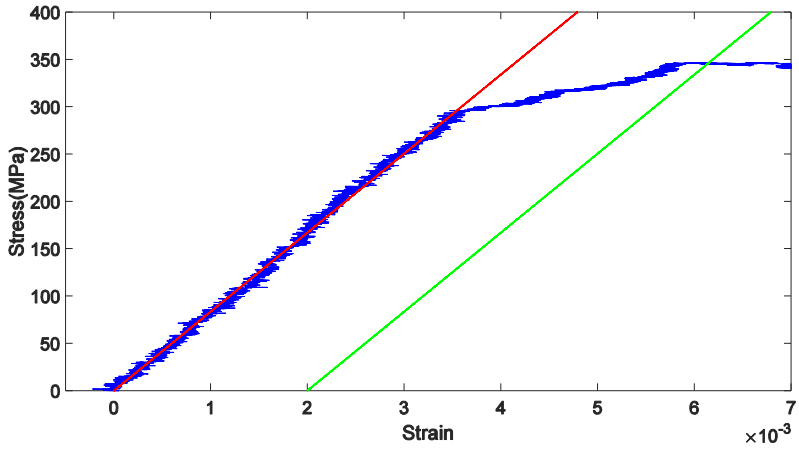

The summary of results of compression tests are given in table 2 below. The Young's modulus of 101 GPa is significantly smaller than the reference value of 138 GPa [18]. Young's modulus has to be the same for all copper specimen regardless of size. This means there could be some systematic errors associated with the experiment. Since both 500 nm and 1 µm copper nanopillars are fabricated on the same copper substrate, the Young's modulus for 1 µm copper nanopillars should be 150 GPa as well. This assertion is also confirmed by DMA tests on 1 µm copper nanopillars (see section 3.4.3) where Young's moduli were found to be 150 GPa for a large number of pillars. The experimental yield strength is in fairly good agreement with the reference value of 300 MPa [20].

Table 2: results for compression tests on 1 µm copper nanopillars

Young's modulus(GPa)	101 ± 5
Yield strength(MPa)	339 ± 15
Diameter(nm)	1024 ± 6
Height(nm)	2903 ± 14

3.2.3 500 nm Fused Silica Nanopillars

No dislocation burst is expected for fused silica nanopillars because there is no dislocation present in amorphous materials. In addition, since fused silica is a brittle material, there is no yielding—only fracture. Loading functions were designed to reach the maximum load of 100 μN or stress of approximately 510 MPa for 500 nm nanopillars which is far below the compressive strength of 1450 MPa [21], or otherwise the pillar fractured. A selected elastic loading plot is shown in figure 16.

Figure 16: the stress vs. strain plot for a uniaxial compression test on a 500 nm fused silica nanopillar

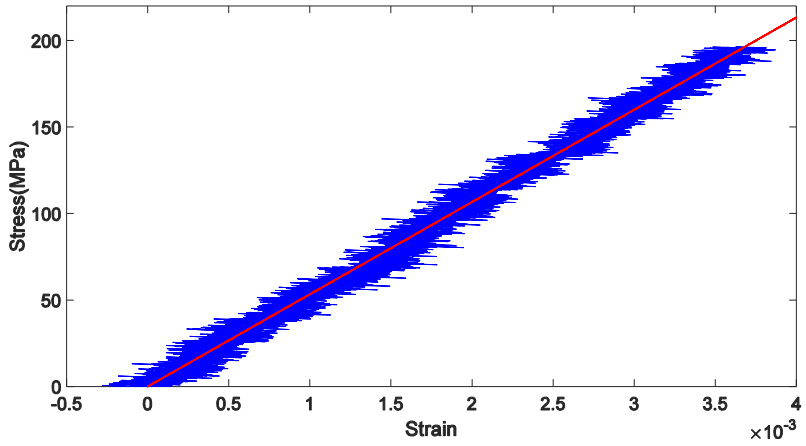

The summary of results of compression tests are given in table 3 below. The reference value for the Young's modulus of fused silica is 71.5 GPa [22]. It was, however, found that the experimental value is significantly smaller than the reference value.

Table 3: results for compression tests on 500 nm fused silica nanopillars

Young's Modulus(GPa)	55.4 ± 0.7
Diameter(nm)	496 ± 3
Height(nm)	1690 ± 80

3.3 Standard Linear Model of Solids

3.3.1 Deduction of Parameters

In order to deduce the outcomes of the dynamic moduli vs. static stress behaviour from the standard linear model of solids, the parameters of the nanoindentation system have to be found first. The meanings of each of the parameters can be found in section 2.7.

These parameters can be found from air indentation (nanoDMA calibration) of the TriboIndenter® mounted with an 8 μm flat diamond punch:

$$k_s = \text{leaf spring stiffness} = 352\ \text{Nm}^{-1}$$

$$m = \text{indenter mass} = 505\ \text{mg}$$

$$D_m = \text{machine damping} = 0.063\ \text{kgs}^{-1}$$

And the other three parameters can be found rigorously using the method described in Wright *et al* (2007) [16]. However, since we are not really interested in the precise values predicted by the model but rather in the overall trend of dynamic moduli vs. static stress, it is not necessary to find these parameters exactly. Instead, the values were obtained by rough estimations with appropriate arguments as followed:

$$k_1 = \text{combined stiffness} = 5.5 \times 10^5\ \text{Nm}^{-1}$$

$$k_2 = \text{material stiffness} = 18300\ \text{Nm}^{-1}$$

$$D_c = \text{contact damping} = 0.01\ \text{kgs}^{-1}$$

The combined stiffness k_1 is estimated by solely taking the indenter stiffness k_i that can be calculated using the equation below:

$$k_i = \frac{2E_i}{1-\nu_i^2}\sqrt{\frac{A_c}{\pi}} \qquad \text{(Eq.6)}$$

where E_i is the Young's modulus of the indenter material, ν_i is the Poisson's ratio of the indenter material, and A_c is the contact area [23]. For diamond E_i and ν_i are 1100 GPa and 0.07 respectively [16]. And A_c is 1.96×10^{-13} m^2 for 500 nm nanopillars.

The material stiffness k_2 can be approximated using the definition of Young's modulus for uniaxial loading:

$$k_2 = \frac{E \times Area}{Height} \qquad \text{(Eq.7)}$$

where *Area* is 1.96×10^{-13} m^2 and *Height* is 1500 nm for 500 nm copper nanopillars.

Lastly, the contact damping is assumed to be as low as the order of magnitude of the machine damping D_m. So it is estimated to be 0.01 kgs^{-1}.

3.3.2 Prediction of Dynamical Behaviour

A Matlab code for finding the predicted displacement from real load data was developed according to the standard linear model of solids (see section 2.7 and A1); and the dynamic moduli vs. static stress behaviour can be deduced accordingly.

However, since later on we will be comparing the behaviour of different materials namely copper and fused silica, it is more useful to replace *storage modulus* and *loss modulus* with *amplitude* and *phase* for the vertical axes.

Amplitude is Young's modulus which is simply the complex modulus of dynamic moduli. With regard to equation 4, storage modulus contains the cosine of phase term which means given that the phase is small, the storage modulus more or less corresponds to the Young's modulus; and that any small variation in the phase does not significantly contribute to the variation in the cosine and thus in the storage modulus itself. Hence, the amplitude vs. static stress behaviour observed also corresponds the storage modulus vs. static stress behaviour.

Phase is the phase by which stress leads strain. In contrast to storage modulus, loss modulus contains the sine of phase term which means given that the phase is small, the variation in the phase, albeit small, can significantly contribute to the variation in the loss modulus as well. Therefore, the phase vs. static stress behaviour observed also corresponds the loss modulus vs. static stress behaviour.

The plots showing *amplitude and phase vs. static stress* for frequencies 1, 10, and 200 Hz are given in figures 17, 18, and 19 respectively. It can be seen that both amplitude and phase are independent of static stress for all frequencies. The error bars come from the errors of fitting real load data to the sloping sinusoid form.

However, the values of amplitude and phase are dependent on frequency. The amplitudes for 1 and 10 Hz are almost identical with the value of approximately 138 GPa but that for 200 Hz is 132 GPa. The phases at all frequencies are very small with the values 0.0014°, 0.0145°, and -0.0066° for 1, 10, and 200 Hz respectively.

These results are based on copper; and the results are identical for both 500 nm and 1 μm nanopillars given that they have the same aspect ratio (1:3 in this project). However, these results can be inferred for fused silica as well by assigning an appropriate value of material stiffness k_2. The only difference is in the values of amplitude and phase, but they are also independent of static

stress. However, the exact values are not of great concern here because they are only estimates, and what is more important is the overall trend.

Figure 17: the amplitude and phase vs. static stress plots for copper nanopillars based on the standard linear model of solids at frequencies 1 Hz

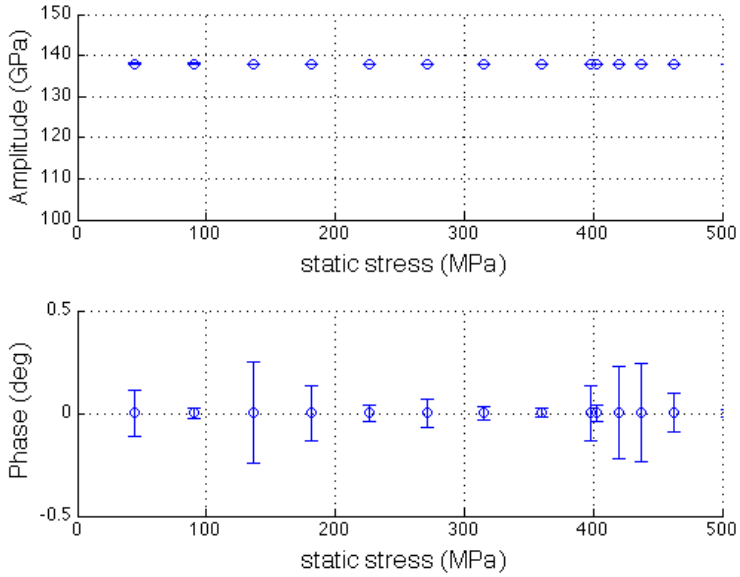

Figure 18: the amplitude and phase vs. static stress plots for copper nanopillars based on the standard linear model of solids at frequencies 10 Hz

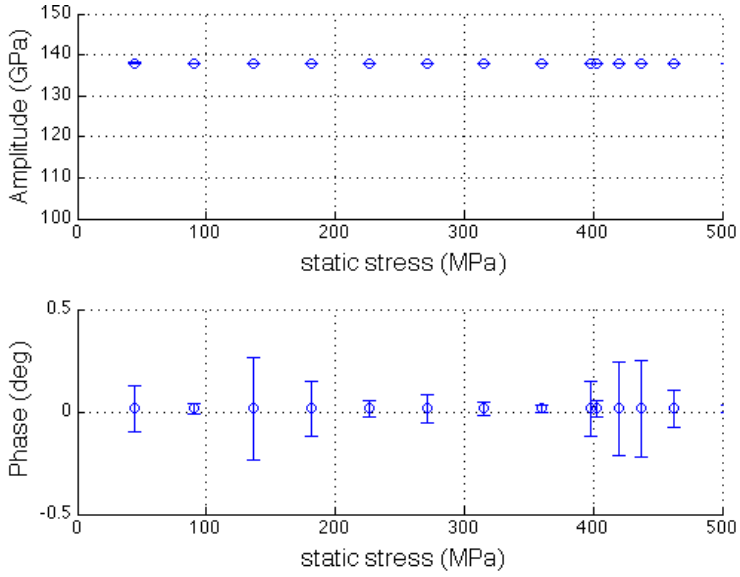

Figure 19: the amplitude and phase vs. static stress plots for copper nanopillars based on the standard linear model of solids at frequencies 200 Hz

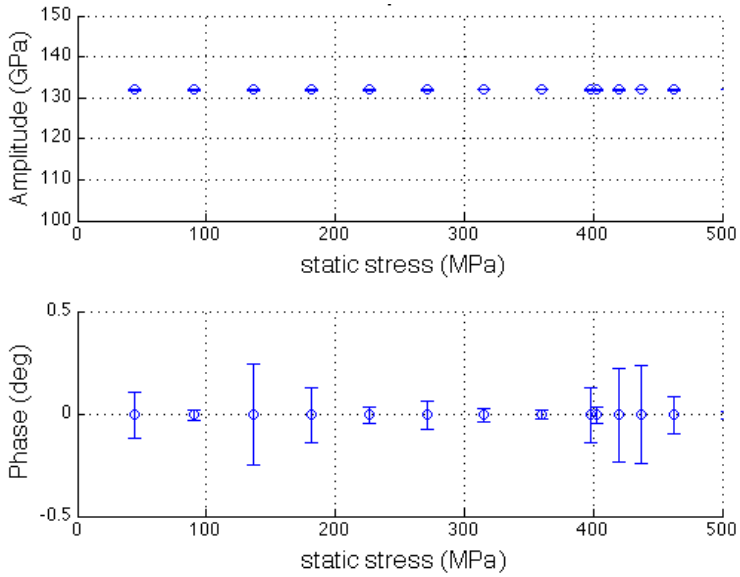

3.4 DMA Tests

3.4.1 Matlab Code for Analysing DMA Test Data

Author's mentor, Xiaoyue, developed a Matlab code for analysing DMA test data. Basically, the code automatically distinguishes the AC segments from raw load and displacement data using the Monte Carlo technique; then, the AC segments are fitted to a sloping sinusoidal function using the method of chi-squared fitting and then the amplitude and phase of load and displacement can be found. Next, the amplitude and phase are plotted versus static stress. Error bars come from the errors of chi-squared fitting.

3.4.2 500 nm Copper Nanopillars

Firstly, we will discuss parameter selection and adjustment for *step* DMA which was used for frequency 1 Hz only. The summary of the parameters for 500 nm copper nanopillars can be found in table A2(a) in section A2 of the appendix.

For most pillars, the maximum load was taken to be 140 μN or equivalent stress of approximately 710 MPa for 500 nm pillars. This was to ensure that the yield point (~540 MPa) was surpassed and the pillars were ultimately plastically deformed. Dislocation bursts were always expected to be observed as an indication of performing a DMA test rather than indentation on the pillar. The number of static steps was chosen from a small value of 14 steps as to see the general outline first before being increased to 16, 20, and 24 steps. The results for 20 and 24 steps have sufficiently good resolution to reveal the dynamical behaviour.

It is stated in section 2.6 that the amplitude of the load should affect the dynamical behaviour. However, it was found in experiment that there is no discernible difference in the dynamical behaviour between difference values of load amplitude (mainly 2 or 4 μN) or even between different types of load amplitude (variable or constant). Selected examples of such dynamical behaviour found in experiment for load frequency 1 Hz are shown in figures 20 and 21.

Figure 20: the amplitude and phase vs. static stress plots for a 500 nm copper nanopillar: 20 steps, frequency 1 Hz, amplitude 4 μN (variable)

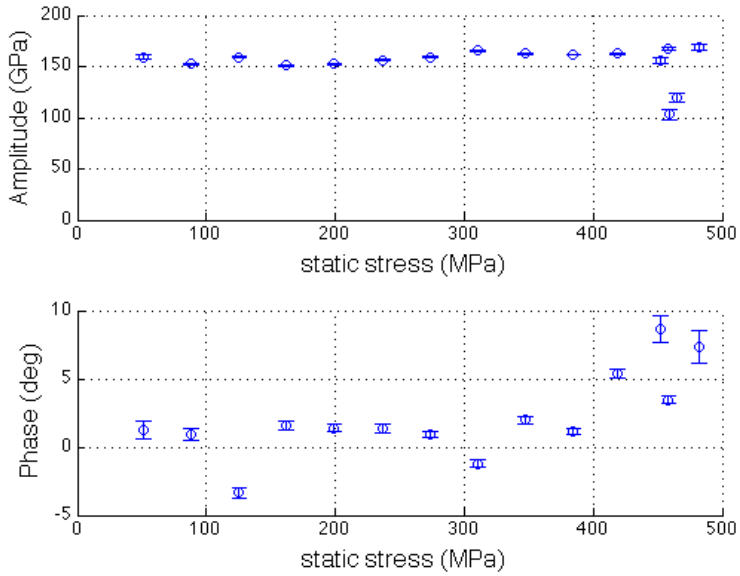

Figure 21: the amplitude and phase vs. static stress plots for a 500 nm copper nanopillar: 24 steps, frequency 1 Hz, amplitude 4 μN (variable)

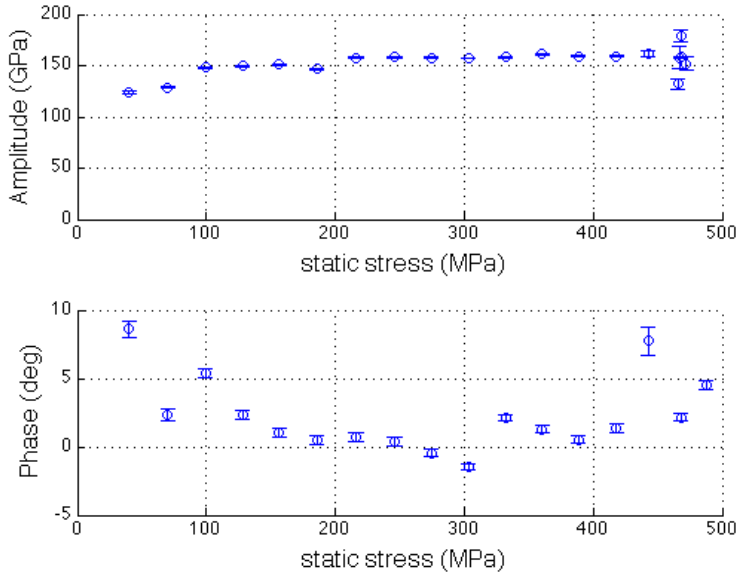

The amplitude (Young's modulus) is fairly constant at the value of approximately 150 GPa which agrees with the benchmark value found in uniaxial compression tests (see table 1). It can be seen that there are some abnormal data points in the high static stress region near the yield point (~500 MPa) that do not fit the trend and possess considerably larger error bars. These data points pertains to the plastic regime so that they can be neglected from the analysis. The trend of *constant* amplitude also agrees with the standard linear model (see figure 17). What is intriguing is that the phase exhibits a significantly *non-constant* trend. This is in contrary to the *constant* phase behaviour predicted by the standard linear model (see figure 17). All of the 500 nm copper nanopillars in the experiment show the *non-constant* phase behaviour but to various extent. For figure 20, there are two obvious minima at around static stress of 125 MPa and 310 MPa. Also notable is that these minima possess negative phase while all other points possess positive phase. A less obvious example is given in figure 21 where the first minima cannot be observed.

Secondly, *continuous* DMA tests were performed for frequency 10 Hz. The maximum load was selected to be 160 μN. The amplitude of the load was all 2 μN (constant). The summary of the parameters for frequency 10 Hz can be found in table A2(b) in section A2 of the appendix. A selected example of the dynamical behaviour is shown in figure 22.

Figure 22: the amplitude and phase vs. static stress plots for a 500 nm copper nanopillar: continuous, frequency 10 Hz, amplitude 2 μN (constant)

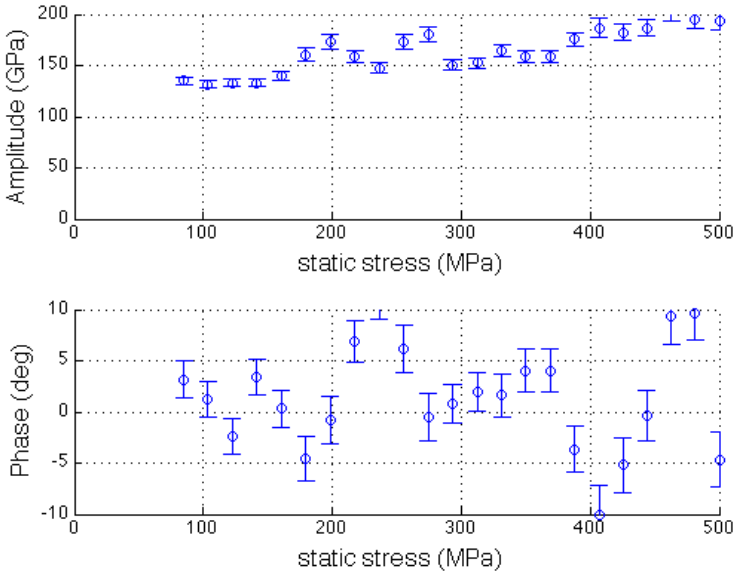

In general, the amplitude is fairly constant at 150 GPa which, again, agrees with the benchmark value. The behaviour of phase is not as well-behaved and obvious as that for frequency 1 Hz; the pattern is rather more random but is, nevertheless, still *non-constant*.

Similarly, *continuous* DMA tests were done for frequency 200 Hz. The maximum load was taken to be 140 μN. The amplitude of the load was all 2 μN (constant). The summary of the parameters

for frequency 200 Hz can be found in table A2(c) in section A2 of the appendix. A selected example of the dynamical behaviour is shown in figure 23.

Figure 23: the amplitude and phase vs. static stress plots for a 500 nm copper nanopillar: continuous, frequency 200 Hz, amplitude 2 μN (constant)

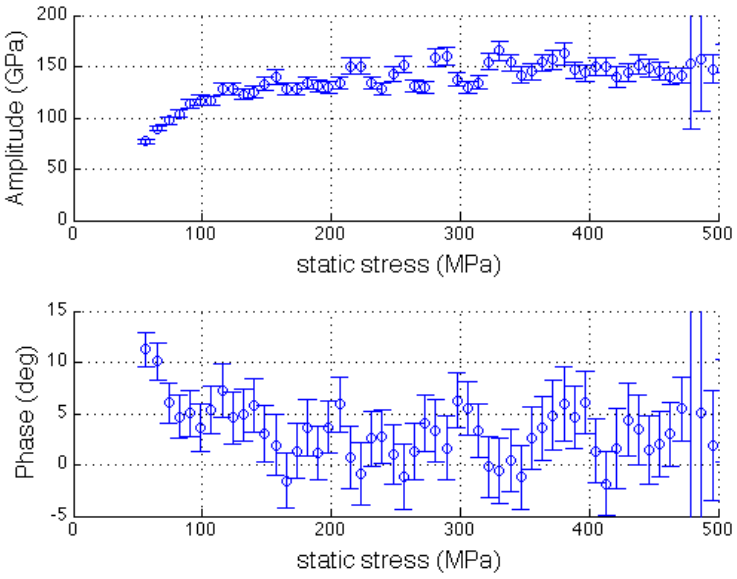

Here, there is a trend of increasing amplitude before saturation to the benchmark value of 150 GPa. This trend is understandable because there could be some softer materials on the top surface of the pillar which means that when the tip is beginning to exert force on the pillar at low static stress values, and these softer materials are being compressed first so that the Young's modulus is smaller than it should be. This kind of behaviour is not uncommon and is observed in a large number of pillars in the experiment. And lastly, the *non-constant* phase behaviour is still observed. Like that of 10 Hz, this *non-constant* phase behaviour looks more random than that of 1 Hz.

3.4.3 1 μm Copper Nanopillars

The parameters for DMA tests are not identical to those of 500 nm nanopillars because different pillar dimensions give rise to different *stiffness.* To achieve the same displacement amplitude, the load amplitude for 1 μm nanopillars must be 3.23 times of that for 500 nm nanopillars. The calculation was based on the actual mean pillar parameters (including Young's modulus, diameter, and height) of the 500 nm and 1 μm copper nanopillars used in experiment.

Firstly, *step* DMA tests were performed for frequency 1 Hz. The summary of the parameters for 1 Hz can be found in table A3(a) in section A3 of the appendix. A selected example of the dynamical behaviour for 1 Hz is shown in figure 24.

Figure 24: the amplitude and phase vs. static stress plots for a 1 µm copper nanopillar: 24 steps, frequency 1 Hz, amplitude 12.92 µN (variable)

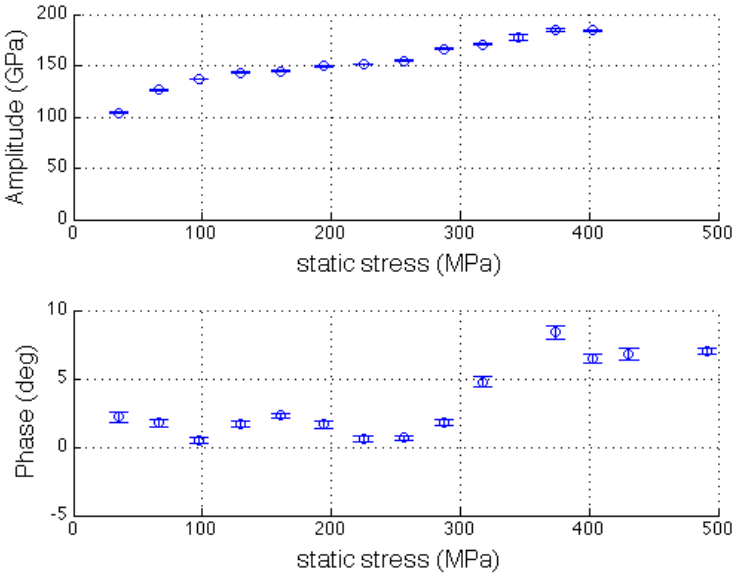

The amplitude shows the same behaviour as that of 500 nm copper nanopillars with the value saturated to 150 GPa. It should be noted that the data points that lie beyond the yield point (~340 MPa) do not fit the trend because they are in the plastic regime and are, hence, not included in the analysis. The *non-constant* behaviour of phase for 1 µm copper nanopillars also recalls that for 500 nm copper nanopillars. The two minima are evident but here they are both positive and the *dip* is of a lesser extent than the case for 500 nm nanopillars (see figure 20).

Secondly, *continuous* DMA tests were performed for frequency 10 Hz just like the tests for 500 nm nanopillars. The summary of the parameters for frequency 10 Hz can be found in table A3(b) in section A3 of the appendix. A selected example is shown in figure 25.

Figure 25: the amplitude and phase vs. static stress plots for a 1 µm copper nanopillar: continuous, frequency 10 Hz, amplitude 4 µN (constant)

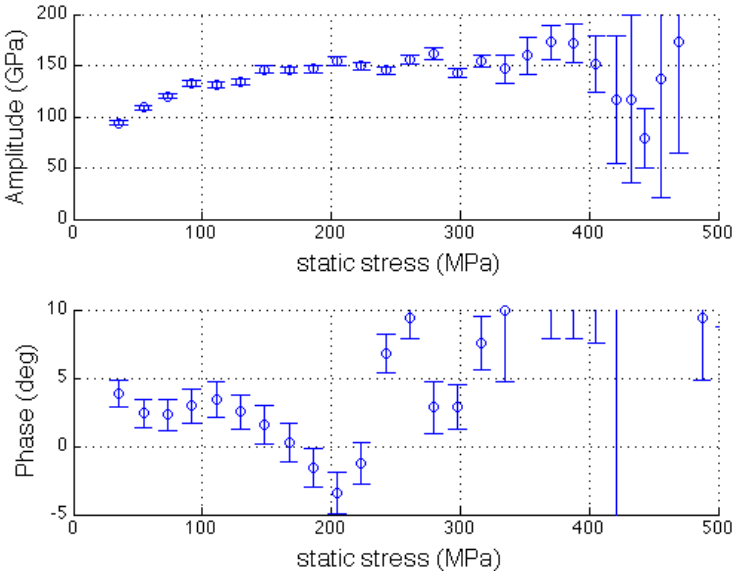

The amplitude shows the common, general trend with the value saturated to 150 GPa as all the others. However, the behaviour of the phase does not quite fit with the others; here there is only one minima at about 200 MPa and then the data points seem to scatter randomly before yielding.

Lastly, similar *continuous* DMA tests were done for frequency 200 Hz. The summary of the parameters can be found in table A3(c) in section A3 of the appendix. A selected example of the dynamical behaviour is shown in figure 26.

Figure 26: the amplitude and phase vs. static stress plots for a 1 μm copper nanopillar: continuous, frequency 200 Hz, amplitude 4 μN (constant)

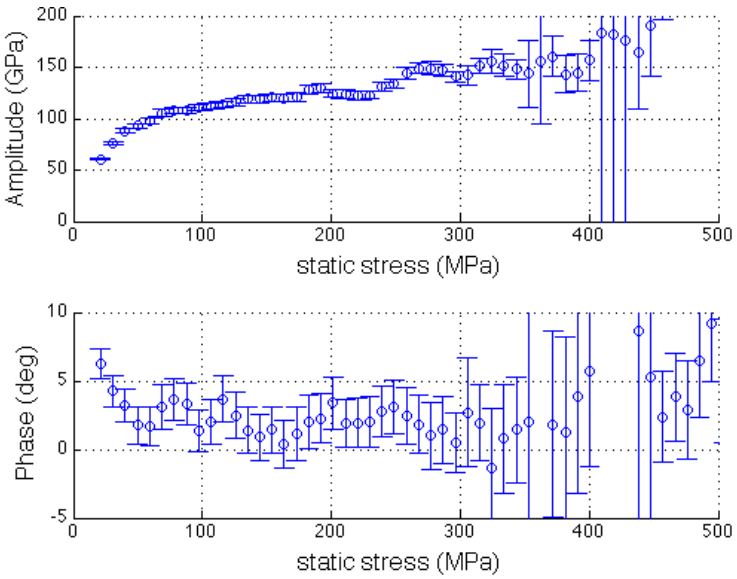

The amplitude here saturates to 125 GPa rather than 150 GPa. However, the amplitude increases again to 150 GPa at the frontier of the elastic regime. And for phase, the *non-constant* behaviour with two minima is observed. But again, the degree to which the minima *dip* is not as high as the case for 500 nm nanopillars.

3.4.4 500 nm Fused Silica Nanopillars

The DMA parameters for 500 nm fused silica nanopillars were chosen as to replicate those for 500 nm copper nanopillars. For 1 Hz, *step* DMA tests were employed. The maximum load is 140 μN or equivalent stress of approximately 710 MPa for 500 nm pillars. This value of stress is still far below the compressive strength of fused silica (~1450 MPa [21]) which means fracture would not occur and the whole range of static stress in the test is elastic. The summary of the DMA parameters can be found in table A4(a) in section A4 of the appendix. A selected example of the result of a step DMA test with frequency 1 Hz on a 500 nm fused silica nanopillar is shown in figure 27.

Figure 27: the amplitude and phase vs. static stress plots for a 500 nm fused silica nanopillar: 14 steps, frequency 1 Hz, amplitude 2 μN (variable)

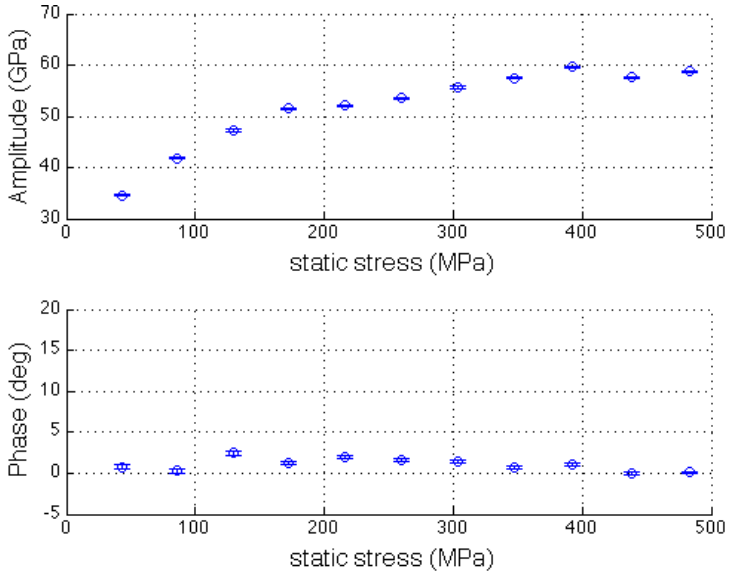

The amplitude begins from a small value before gradually increasing and saturating to the value of approximately 58 GPa. This value is slightly larger than the benchmark value of 55.4 GPa. Unlike its copper counterpart, the phase is fairly constant throughout and therefore agrees with the standard linear model.

Lastly, *continuous* DMA tests were performed for frequencies 10 and 200 Hz. The summary of the parameters for frequencies 10 and 200 Hz can be found in tables A4(b) and A4(c) respectively in section A4 of the appendix. Respective examples are given in figures 28 and 29.

Figure 28: the amplitude and phase vs. static stress plots for a 500 nm fused silica nanopillar: continuous, frequency 10 Hz, amplitude 1 μN (constant)

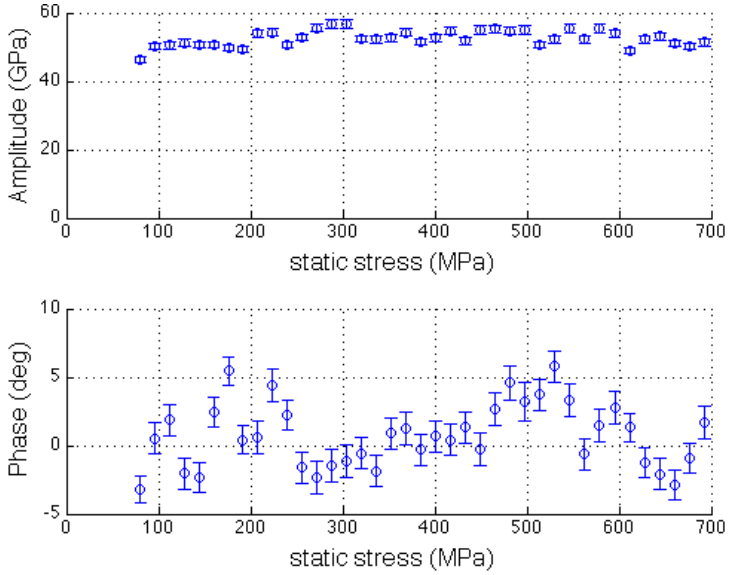

Figure 29: the amplitude and phase vs. static stress plots for a 500 nm fused silica nanopillar: continuous, frequency 200 Hz, amplitude 1 μN (constant)

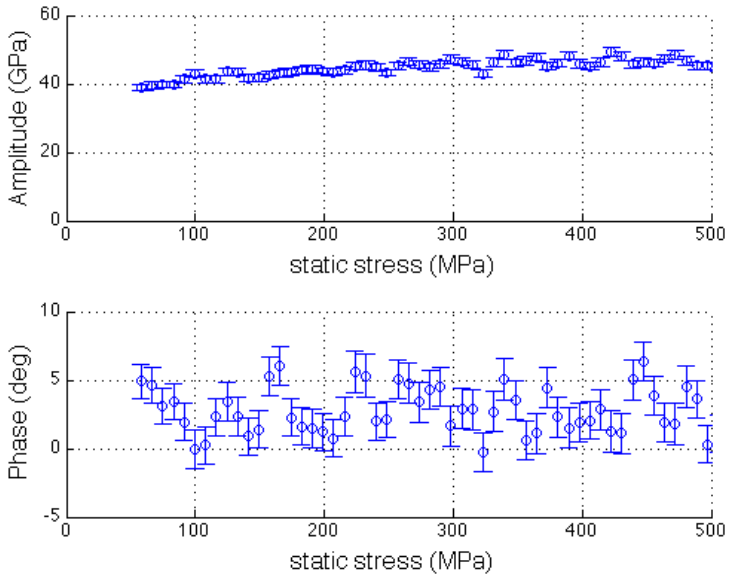

For the amplitude part, the results for both frequencies agree with the benchmark value. However, it can be seen that the behaviour of phase is different from what was found for 1 Hz; here the phase is obviously not constant throughout. This issue is discussed in the next section.

3.5 Discussion

The DMA results for frequency 1 Hz of all the types of pillars are satisfactory and agree with our hypothesis; that is there is a deviation from the linear, elastic picture (standard linear model of solids). It was found that the behaviour of phase (and hence, loss modulus) for copper is different from that for fused silica; *non-constant* versus *constant* phase. And it was found that the extent of this *non-constant* phase (loss modulus) behaviour for 1 μm copper nanopillars is less than that for 500 nm copper nanopillars; in other words, there is *size-dependence.* This evidence might indicate intermittent dislocation dynamics in the elastic regime as proposed in sections 1.3 and 2.8.

In addition, there might be other extrinsic causes of this anomalous behaviour: *machine artefacts* and *calibration*. Firstly, *machine artefacts* in this experiment are specifically artefacts due to *thermal drift* of the nanoindenter. *Thermal drift* is drift in displacement as the indenter tip drifts into or from the surface of the sample due to thermal expansion of the components of the nanoindentation machine [11]. It is most likely to be caused by thermal expansion of the *leaf springs* inside the transducer assembly (see figure 4). The major source of heat is machine damping (D_m), which already incorporates the damping of the leaf springs. However, according to author's calculation, this heat is too minimal to cause any significant thermal expansion even on the nanoscales. Secondly, *calibration* specifically means the calibration for the machine parameters

that are involved in the conversion of voltage into force and displacement. Calibration is performed only at the beginning of the experiment. These parameters might not be constant over the course of the test. However, the variations in the values of the parameters, if any, would be rather random in nature. It was found that the dynamical behaviour found (*non-constant* phase) is consistent for a large number of pillars.

However, for frequencies 10 and 200 Hz, a similar conclusion cannot be made because the patterns of phase for fused silica found in the experiment are also *non-constant*. After thorough revision on the methodology (see section 2.5), it was found that there are some issues with *continuous* DMA per se. There could be variations in the amplitude and phase of each of the sinusoids contained in a *packet* as the test proceeds either from random fluctuations (machine noise) or other intrinsic agents (dislocation mechanics). Since the *overall* amplitude and phase of the *packet* is derived from the *best-fit* amplitude and phase, all the immanent variations are averaged out. Thus, the *overall* amplitude and phase do not represent the true values associated with that value of static stress, which is also an average value.

4. Conclusion

Our experimental results confirm a deviation from the perfectly linear elastic behaviour for copper nanopillars under oscillatory perturbation with frequency 1 Hz. Loss moduli are not constant throughout the static, elastic regime. This anomalous dynamic mechanical behaviour is of a lesser degree for larger systems and this, therefore, indicates size-dependence of the behaviour. This serves as evidence for non-trivial microstructure evolution and might further indicate intermittent dislocation dynamics in the elastic regime as the source of crackling noise. However, this still requires a further theoretical model to describe the observed behaviour. Further experimental work is also required to test the frequency-dependence of this behaviour.

Acknowledgements

I would like to thank Xiaoyue for all her help on my project from the very beginning to the end of summer. I have learned a lot of things from her this summer. Also I would like to thank all my fellow LIGO and other summer students for their support and cordiality. This project was kindly funded by the National Science Foundation and California Institute of Technology under the LIGO Summer Undergraduate Research Fellowship programme 2015.

References

[1] M. Willcox, T. Mysak. (2004). *An Introduction to Barkhausen Noise and its Applications*. InsightNDT Equipment.

[2] E. Quintero, E. Gustafson, R. Adhikari. (2013). *Experiment to Investigate Crackle Noise in Maraging Steel Blade Springs*. LIGO.

[3] C. Hamil, G. Vajente, E. Quintero. (2015). *An Optical Setup for Crackle Noise Detection.* LIGO.

[4] X. Ni, E. Quintero, G. Vajente. (2015). *Proposal for an upgrade of the Crackle experiment*. LIGO.

[5] M. Meyers, K. Chawla. (2009). *Mechanical Behaviours of Materials*. Cambridge University Press.

[6] L. Laurson, M.J. Alava. (2012). *Dynamic Hysteresis in Cyclic Deformation of Crystalline Solids*. Phys. Rev. Lett. 109, 155504.

[7] J.R. Greer, J.Th.M. De Hosson. (2011). *Plasticity in small-sized metallic systems: Intrinsic versus extrinsic size effect.* Prog Mater Sci. 56(6), 654-724.

[8] A. Latif. (2000). *Nanofabrication Using Focused Ion Beam* (Doctoral dissertation). Retrieved from https://www.repository.cam.ac.uk/bitstream/handle/1810/34605/Latif_thesis.pdf?sequence=3

[9] N. Yao. (2011). *Focused Ion Beam Systems: Basics and Applications*. Cambridge University Press.

[10] FEI Company. (2011). *Product Data for FEI™ Versa 3D™*. Retrieved from http://www.microscop.ru/uploads/VERSA3D.pdf

[11] A.C. Fischer-Cripps. (2002). *Nanoindentation* .Springer Science+Business Media.

[12] Hysitron Inc. *Nanoscale Indentation: an Overview of Hysitron Quasistatic Nanoindentation*. Retrieved from https://www.hysitron.com/media/1678/nanoindentation-1.pdf

[13] Hysitron Inc. *Rigid Probe Indentation: Comparison of Hysitron TriboIndenter®/TriboScope® and AFM-based Nanoindentation*. Retrieved from https://www.hysitron.com/media/1679/nanoindentation-2.pdf

[14] Hysitron Inc. (2001). *TriboIndenter® User's Manual.*

[15] X. Ni. (2015). *What is Crackling Noise: a Study of Micro-mechanics of Flow in Metals* (Presentation poster). LIGO.

[16] W.J. Wright, A.R. Maloney, W.D. Nix. (2007). *An Improved Analysis for Viscoelastic Damping in Dynamic Nanoindentation*. Int. J. Surface Science and Engineering, Vol. 1, Nos. 2/3, 274–292.

[17] API. (2004) *SPEC 16A, Specification for Drill-through Equipment, Third Edition.*

[18] Y. Gao, H. Wang, J. Zhao, C. Sun, F. Wang. (2011) *Anisotropic and Temperature Effects on Mechanical Properties of Copper Nanowires under Tensile Loading*. Comput. Mater. Sci. 50 (10), 3032-3037.

[19] D. Jang, C. Cai, J.R. Greer. (2011). *Influence of Homogeneous Interfaces on the Strength of 500 nm Diameter Cu Nanopillars*. Nano Lett. 11 (4), 1743-1746.

[20] A.T. Jennings, M.J. Burek, J.R. Greer. (2010). *Microstructure versus Size: Mechanical Properties of Electroplated Single Crystalline Cu Nanopillars*. Phys. Rev. Lett. 104, 135503.

[21] F. Cardarelli. (2008). *Materials Handbook: a Concise Desktop Reference, Second Edition*. Springer Science+Business Media.

[22] L. Zheng, A.W. Schmid, J.C. Lambropoulos. (2007). *Surface Effects on Young's Modulus and Hardness of Fused Silica by Nanoindentation Study*. J. Mater. Sci. 42 (1), 191-198.

[23] W.C. Oliver, G.M. Pharr. (1992). *An Improved Technique for Determining Hardness and Elastic Modulus Using Load and Displacement Sensing Indentation Experiments*. J. Mater. Res. 7 (6), 1564-1583.

Appendix

A1. Standard Linear Model of Solids

With regard to Wright *et al* (2007) [16], modelled displacement can be calculated from AC load data of the sloping sinusoid form as followed:

$$F_{app} = c_F + m_F t + F_0 \sin(\omega t + \psi_F)$$

where
F_{app} = load
t = time
c_F = y-intersection
m_F = slope
F_0 = amplitude
ω = angular frequency
ψ_F = initial phase

The resultant displacement u of the same form is the solution (particular integral) to the differential equation governing the system (not shown here because of its lengthiness):

$$u = c_u + m_u t + u_0 \sin(\omega t + \psi_u)$$

It was found that:

$$c_u = \frac{c_F + m_F(B - \frac{A}{G})}{G}$$

$$m_u = \frac{m_F}{G}$$

$$u_0 = F_0 \sqrt{\frac{1 + (\omega B)^2}{[G - \omega^2(H + m)]^2 + [\omega A - \omega^3 BM]^2}}$$

$$\psi_u = \psi_F + \tan^{-1}(\omega B) - \tan^{-1}(\frac{\omega A - \omega^3 Bm}{G - \omega^2(H + m)})$$

where
$A = \left(\frac{k_1 + k_s}{k_1 + k_2}\right) D_c + D_m$
$B = \frac{D_c}{k_1 + k_2}$
$G = k_s + \frac{k_1 k_2}{k_1 + k_2}$
$H = \frac{D_c D_m}{k_1 + k_2}$

These coefficients characterise the whole system of both the material and the indenter itself. Load leads displacement by:

$$\delta = \psi_F - \psi_u = \tan^{-1}\left(\frac{\omega A - \omega^3 Bm}{G - \omega^2(H+m)}\right) - \tan^{-1}(\omega B)$$

Dynamic stiffness is defined as:

$$\frac{F_0}{u_0} = \sqrt{\frac{[G - \omega^2(H+m)]^2 + [\omega A - \omega^3 Bm]^2}{1 + (\omega B)^2}}$$

Complex dynamic modulus is defined as:

$$E = E_{storage} + iE_{loss} = \frac{F_0}{u_0} \times \frac{Height}{Area} \times \exp(i\delta)$$

Since both dynamic stiffness and phase difference have no dependence on c_F, or in other words they do not depend on the static load of each load step, dynamic moduli must be constant throughout the elastic loading regime at constant frequency.

A2. DMA Parameters: 500 nm Copper Nanopillars

Table A2(a): summary of the parameters for step DMA tests on 500 nm copper nanopillars with frequency 1 Hz

Steps	Maximum Load/μN	Begin Amplitude/μN	Amplitude Type	Number of pillars done
14	140	2	variable	2
14	140	4	variable	4
14	140	8	variable	2
16	140	2	variable	2
16	140	4	variable	2
16	140	8	variable	2
16	140	1	variable	3
20	140	2	variable	3
20	140	2	constant	2
20	140	4	variable	2
20	140	4	constant	2
24	140	2	variable	2
24	140	2	constant	2
24	140	4	variable	2
24	140	4	constant	2

Table A2(b): summary of the parameters for continuous DMA tests on 500 nm copper nanopillars with frequency 10 Hz

Maximum Load/μN	Amplitude/μN	Amplitude Type	Number of pillars done
160	2	constant	9

Table A2(c): summary of the parameters for continuous DMA tests on 500 nm copper nanopillars with frequency 200 Hz

Maximum Load/μN	Amplitude/μN	Amplitude Type	Number of pillars done
140	2	constant	9

A3. DMA Parameters: 1 μm Copper Nanopillars

Table A3(a): summary of the parameters for step DMA tests on 1 μm copper nanopillars with frequency 1 Hz

Steps	Maximum Load/μN	Begin Amplitude/μN	Amplitude Type	Number of pillars done
24	604.8	6.46	variable	2
24	604.8	6.46	constant	2
24	604.8	12.92	variable	2
24	604.8	12.92	constant	2

Table A3(b): summary of the parameters for continuous DMA tests on 1 μm copper nanopillars with frequency 10 Hz

Maximum Load/μN	Amplitude/μN	Amplitude Type	Number of pillars done
605	4	constant	6

Table A3(c): summary of the parameters for continuous DMA tests on 1 μm copper nanopillars with frequency 200 Hz

Maximum Load/μN	Amplitude/μN	Amplitude Type	Number of pillars done
605	4	constant	6

A4. DMA Parameters: 500 nm Fused Silica Nanopillars

Table A4(a): summary of the parameters for step DMA tests on 500 nm fused silica nanopillars with frequency 1 Hz

Steps	Maximum Load/μN	Begin Amplitude/μN	Amplitude Type	Number of pillars done
14	140	2	variable	4
14	140	4	variable	4
16	140	2	variable	2
16	140	4	variable	2
20	140	1	constant	6

Table A4(b): summary of the parameters for continuous DMA tests on 500 nm fused silica nanopillars with frequency 10 Hz

Maximum Load/μN	Amplitude/μN	Amplitude Type	Number of pillars done
140	1	constant	6

Table A4(c): summary of the parameters for continuous DMA tests on 500 nm fused silica nanopillars with frequency 200 Hz

Maximum Load/μN	Amplitude/μN	Amplitude Type	Number of pillars done
140	1	constant	6